JOURNAL OF Materials CHEMISTRY

Crystal structure and characterisation of cadmium cyanamide

Gianguido Baldinozzi,[a] Barbara Malinowska,*[b] Mohammed Rakib[b] and Gérard Durand[b]

[a]*Laboratoire Structures, Propriétés et Modélisation du Solide, Ecole Centrale Paris, Grande Voie des Vignes, Châtenay-Malabry Cedex, France F-92295*
[b]*Laboratoire de Chimie et Génie des Procédés, Ecole Centrale Paris, Grande Voie des Vignes, Châtenay-Malabry Cedex, France F-92295. E-mail: malinows@cgp.ecp.fr*

Received 20th July 2001, Accepted 24th October 2001
First published as an Advance Article on the web 19th December 2001

The crystal structure of cadmium cyanamide was investigated by X-ray powder analysis and refined using the Rietveld method. Very fine powders of $CdCN_2$ in the nanometre range were obtained by chemical bath deposition. The size, shape and microstrain were characterised by X-ray diffraction and transmission electron microscopy. The refined structure is very close to that of $MgCN_2$. Infrared spectroscopy and thermogravimetric analysis were also performed to fully characterise the compound.

Introduction

The first reference to cadmium cyanamide is given by Bolis-Cannella[1] who performed a thermogravimetric analysis under ambient air or nitrogen. He precipitated $CdCN_2$ as a white powder by reaction of cyanamide (H_2CN_2) with cadmium acetate in 10% NH_3 solution. Later, in the 1970s, cadmium cyanamide was identified in the bulk precipitate and in CdS films obtained on glass by Chemical Bath Deposition (CBD).[2,3] Consequently $CdCN_2$ was separately synthesised[4] and first analysed by infrared spectroscopy and XRD.[2,5] The authors used a solution of H_2CN_2 together with a solution of cadmium chloride in the presence of ammonia for a precipitation reaction. More recently, a growing interest in cadmium cyanamide has been noticeable due to the presence of carbon–nitrogen impurities in the CdS layer both in CdTe- and in Cu(In,Ga)Se_2-based thin-film solar cells.[6–8] One of the possible reasons for these impurities is the formation of cadmium cyanamide.[7]

This study is part of the work on deposition of CdS thin films by the CBD method.[9–11] For the first time we have obtained a new crystalline phase of $CdCN_2$ different from that already reported by Dvoinin *et al.*[5] We have characterised this phase by X-ray powder diffraction (XRPD), transmission electron microscopy (TEM), infrared spectroscopy (FTIR) and thermogravimetric studies (TG–DSC).

Experimental

Cadmium cyanamide was prepared starting from $CdCl_2{\cdot}2.5H_2O$ (p. a. Acros, 28 g) and ammonia (RPE reagenti, Carlo Erba, about 70 cm^3 of 30% NH_3). $CdCl_2$ is firstly dissolved in de-ionised water. Then, ammonia is added to the solution. At the beginning of this reaction, cadmium hydroxide is deposited but it disappears as soon as an excess of NH_3 is added. Sodium hydroxide (98%, Labosi, 0.23 g) is then added for the optimisation of pH and the solution is made up with water to 250 cm^3. The optimum pH for the reaction is in the range 12.2–12.5. This solution is subsequently heated in a sealed round-bottomed flask at 348 K. Then cyanamide H_2CN_2 (99%, Aldrich, 150 cm^3 of 0.9 M solution in water) is added to the flask. A white cadmium cyanamide precipitate is formed. Heating at 348 K is maintained for 15 minutes, followed by natural cooling at room temperature. Very fine $CdCN_2$ powder is obtained. The use of a 0.7 μm cut-off filter is needed to separate the precipitate from the aqueous solution.

Methods

X-Ray diffraction

XRD patterns were collected in Bragg–Brentano geometry on a prototype diffractometer[12] equipped with a graphite monochromator on the detector arm. Cu-Kβ radiation was selected to obtain a simple profile for the Rietveld refinement. Because of the crystallite characteristics, particular attention was paid during the sample preparation in order to reduce any preferential crystallite orienting. Since the grain size is very small and almost monodispersed, there was no need to use a mesh to obtain a uniform granularity. The powder diffraction patterns are recorded with an accurate temperature control (use of a gas cooled cryostat at 294 K). The sample temperature was kept stable within an interval of 0.5 K. The diffraction pattern was collected during multiple scans until the counting statistic was considered satisfactory. The multiple scans were then rebinned to obtain a single diffraction pattern with the proper statistical weights for each point. The diffraction pattern was then refined using the Rietveld program XND.[13]

Transmission electron microscopy

TEM observations were carried out with a JEOL JEM 1200EX instrument. The ethanol suspension of the powder was deposited on carbon coated copper grids to insure a good electrical conductivity. The samples were examined at 120 kV.

Thermal analysis (TG–DSC)

Thermogravimetry (TG) coupled with differential scanning calorimetry (DSC) was performed with a Setaram TGA92 under a stream of oxygen heating and cooling in the temperature range 300–1100 K. A sample mass of 16 mg was put in an alumina sample holder and an equivalent mass of corundum was used as reference. The rates of heating and cooling were 5 K min^{-1}.

Infrared scattering

FTIR spectra were recorded with a Bruker IFS66 spectrometer in the wavenumber range 400–4000 cm^{-1}. The sample is obtained by mixing 1 mg of fine powder of $CdCN_2$ with 100 mg of KBr to insure a good signal to noise ratio. The mixture is then pressed to form a disk. The infrared spectrum was obtained from an accumulation of 50 scans collected with a 4 cm^{-1} resolution.

 DOI: 10.1039/b106498c

This journal is © The Royal Society of Chemistry 2002

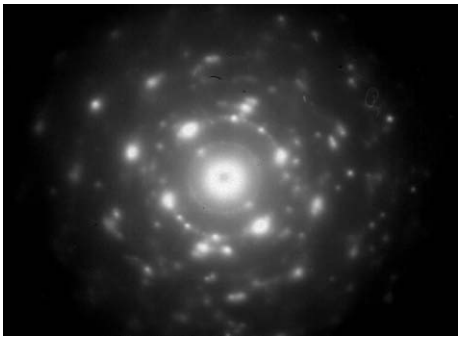

Fig. 1 ED diffraction pattern for a synthesised $CdCN_2$ sample.

Fig. 2 Transmission electron micrograph of the $CdCN_2$ particles.

Elemental analysis

This was performed with Elemental Analyser NCS2500 in order to determine the elemental composition of the compound. The process is known as Dynamic Flash Combustion. We determined in a single analysis nitrogen and carbon while cadmium was deduced by difference. The sample masses were approx. 2–3 mg. Elemental composition found: N, 18.12%, C, 7.65% and Cd, 74.23%.

Results and discussion

TEM observations

We have analysed the diffraction patterns collected on nanocrystalline powders. The various electron diffraction patterns mainly correspond to the 00l zone axis (Fig. 1). All the diffraction spots can be indexed according to the space group derived from the analysis of the X-ray powder diffraction patterns. We have tried to obtain high resolution images of the nanopowders but the sample is not stable under the electron beam and focusing the beam invariably leads to the destruction of the sample. Therefore, it was possible to obtain good images at an average resolution only in few cases. These images reveal crystallites having a very complex shape (Fig. 2). The measured size and shape of the crystallites are in very good agreement with the X-ray model for the lineshape broadening produced by the finite size and microstrain effects.

Analysis of line widths

It was possible to index the diffraction pattern using a trigonal *R* centred lattice ($a = 3.5317(1)$ Å, $c = 14.5558(4)$ Å at 294 K).

The profiles of the peaks in the high resolution X-ray diffraction patterns present a complex broadening due to size or strain effects. In order to determine the reasons for this anisotropic broadening, we have measured the width at half maximum of the different peaks. The angular dependence of the widths is best displayed using a Williamson–Hall plot.[14]

As can be seen in the Williamson–Hall plot (Fig. 3), all peaks are affected both by a size broadening and a strain broadening. The size of the coherent diffracting domains in Å, along a given direction, is obtained by the reciprocal of the intercept of the linear regressions at the *y* axis while the strain effect is given by the slope of these regression lines. The common feature of the diagram is that the strain component is almost isotropic since the slopes of the different regression lines are almost equal. On the other hand, the coherent diffracting domains have a rather complex shape. The largest diameters are along the 00l threefold axis (where the broadening is almost instrumental) and along the directions *hk*0, normal to this axis. The size of the coherent diffracting domains along the *c* axis is 630 Å while it is

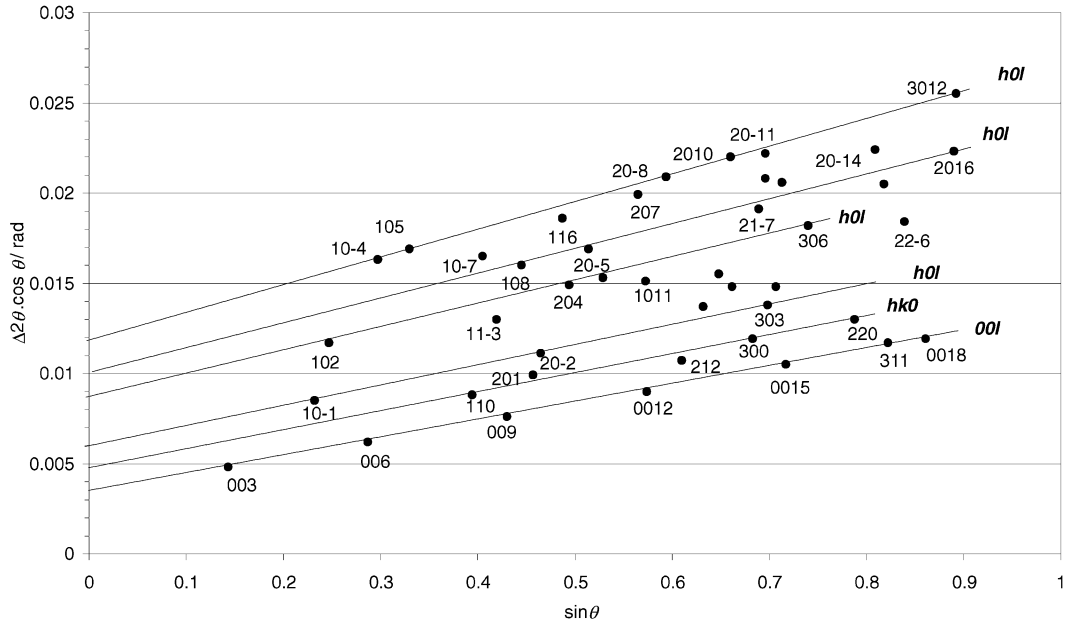

Fig. 3 A Williamson–Hall plot for the crystallite of $CdCN_2$.

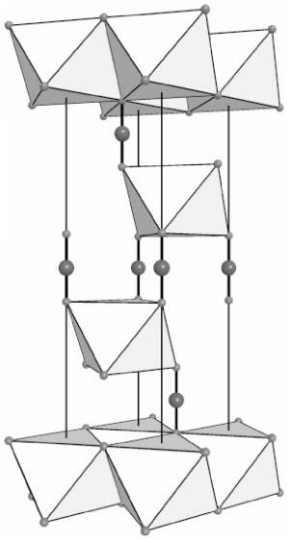

Fig. 4 Representation of the average structure of $CdCN_2$. C is shown as large grey spheres that are two coordinate with nitrogen. Cd is sitting at the centre of the N6 octahedra.

450 Å in the hexagonal plane. The minimum size (130 Å) for the coherent domains is reached for directions far from both the trigonal axis and the hexagonal plane. On the other hand, the diffraction peaks are almost symmetrical (they only present a weak instrumental asymmetry), suggesting a normal dispersion for the domain sizes.

Structure refinement

Since no systematic extinction is observed in the indexed diffraction pattern and the lattice metric is trigonal, the space group was supposed to be $R\bar{3}m$. It is interesting to point out that one other cyanamide compound crystallises within this space group, ($MgCN_2$) as described by Berger and Schnick.[15]

Therefore we have taken the structure of this compound as an initial guess for refining the $CdCN_2$ structure. The crystal structure of $CdCN_2$ can be viewed as an ionic layered structure consisting of layers of edge-sharing CdN_6 octahedra. These slabs are then connected together by C atoms so that alternating layers of anions and cations are stacked along the *c*-axis (Fig. 4).

As we have discussed in the previous section, the diffraction peaks exhibit an anisotropic broadening. In order to obtain a reliable estimate for the integrated intensities, we have taken into account these anisotropic lineshapes of the diffraction peaks. The structural parameters and the results of the Rietveld refinement are satisfactory and they are summarised in Tables 1 and 2.

Table 1 Cell parameters and reliability factors for the $CdCN_2$ structure at 294 K

	294 K	294 K
Crystal system	Trigonal	Trigonal
Space group	$R\bar{3}m$ (no 166)	$R3m$ (no 160)
Formula weight	152.4	
Volume/Å^3	157.28(5)	
Density calc./g cm^{-3}	4.827	
Z	3	
2θ range/°	14–133	
Wavelength/Å	Cu Kβ = 1.39223	
a/Å	3.5316(9)	3.5321(7)
c/Å	14.555(5)	14.557(4)
Observed reflections	131	131
R_{wp}(%)	10.11	9.99
R_I(%)	4.55	4.45
R_F(%)	3.30	3.31

Table 2 Positional and anisotropic displacement parameters for $CdCN_2$ at 294 K in the $R\bar{3}m$ space group. Because of the site symmetries, $U^{11} = U^{22} = 0.5*U^{12}$ and $U^{23} = U^{13} = 0$. The thermal displacement parameters of C and N were constrained to be equal

	Site	x	y	z	U^{11}	U^{33}
Cd	3a	0	0	0	0.0034(5)	0.0193(10)
C	3b	0	0	½	0.0010(20)	0.086(8)
N	6c	0	0	0.4175(7)	0.0010(20)	0.086(8)

One interesting point is that, within this space group, the bond lengths between a C atom and the two first-neighbour N atoms belonging to two different anionic layers are identical. Now we can expect that these two C–N bonds would be different since the IR spectra suggest the existence of triple and simple C–N bonds. The thermal ellipsoid of the C atom is actually noticeably elongated along the *c*-axis (the N–C–N bonding direction). Within this model, the two C–N bonds are equivalent and the only way to differentiate them is to reduce the symmetry of the structure. One possibility is to perform the refinement in the $R3m$ space group (*i.e.* removing the inversion centre in the previous space group). It is well known that the refinement of powder data in an acentric space group is very difficult because of peak overlap. Within this group, the two N atoms are no longer symmetry related and two independent N atoms sitting on the threefold axis will be needed to describe the cyanamide structure. The z positions of C, N1 and N2 are in principle free but the simultaneous refinement of these three parameters leads to very large estimated square deviations for the z parameter of N1 and N2. Therefore we have chosen to constrain some of these parameters: we have assumed a symmetric stretching of the N1–N2 distance while letting the C position be unconstrained along the axis. The result of this refinement is summarised in Tables 3 and 4. The observed, calculated and difference patterns are shown in Fig. 5.

Though the reliability factors are only slightly better, this model presents the advantage of giving a more accurate description of the $[N(1)\equiv C-N(2)]^{2-}$ configuration, compatible with our FTIR observations.

FTIR

The FTIR spectrum of cadmium cyanamide shows one strong and broad vibration band with the maximum at 2113 cm^{-1} (Fig. 6a). Within this band, a shoulder is observed at 2071 cm^{-1} (Fig. 6b). On the other hand, the strong vibration band at 655 cm^{-1} is sharp. According to the literature, the

Table 3 Positional and anisotropic displacement parameters for $CdCN_2$ at 294 K in the non centrosymmetric space group $R3m$. Because of the site symmetries, $U^{11} = U^{22} = 0.5*U^{12}$ and $U^{23} = U^{13} = 0$. The thermal displacement parameters of C and N1 and N2 were constrained to be equal

	Site	x	y	z	U^{11}	U^{33}
Cd	3a	0	0	0	0.0033(5)	0.0215(10)
C	3b	0	0	0.489(4)	0.0010(20)	0.085(11)
N1	3b	0	0	0.4176(7)	0.0010(20)	0.085(11)
N2	3b	0	0	0.5824(7)	0.0010(20)	0.085(11)

Table 4 Bond lengths (Å) at room temperature (294 K) according to the refinement of the X-ray diffraction pattern in the $R3m$ space group

Cd–N1	2.380(4)
Cd–N2	2.380(4)
C–N1	1.04(4)
C–N2	1.36(4)
N1–N2	2.400(13)

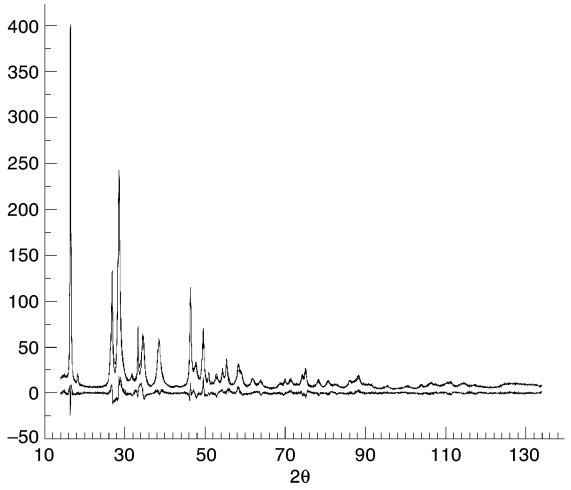

Fig. 5 Experimental, calculated and difference powder XRD patterns for $CdCN_2$. The complex size and strain corrections are the main responsible for the discrepancies between observed and calculated diffraction patterns. The good quality of the structural model is assessed by the low R_I factor.

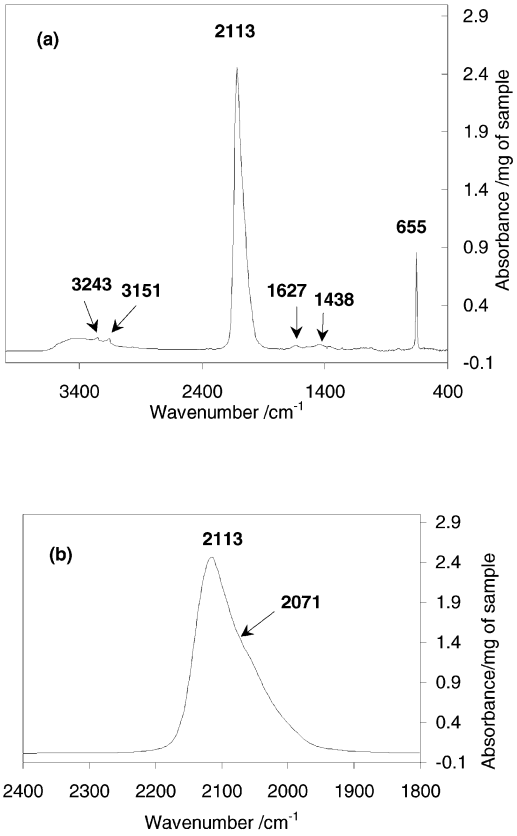

Fig. 6 FTIR spectra of $CdCN_2$: (a) spectrum in the range 400–4000 cm^{-1}, (b) detail of the spectrum above.

absorption band at frequencies close to 2000 cm^{-1} is due to a stretching vibration of the triple bond (C≡N) in the cyanamide ion $[N(2)–C{\equiv}N(1)]^{2-}$ whereas that at 655 cm^{-1} is attributed to the vibration of a simple bond (N–C).[5] Uritskaya *et al.*[2] observed a broad band close to 2000 cm^{-1} while Dvoinin *et al.*[5] noticed two vibration bands in the same frequency range: at 1980 and 2100 cm^{-1}. These authors also observed two bands at 3400 and 1640 cm^{-1} and weak vibration bands at 2860, 3020, 3155, 3250 cm^{-1}. The absorption band in the range 1660–1590 cm^{-1} may be assigned to the existence of H_2O or/and to NH_3 bending modes.[6,16] The broad band between 3700 and 2900 cm^{-1} can also be assigned to the presence of water molecules.[6,16] Other weak bands are related to impurities.

Literature gives many explanations for the splitting at 2000 cm^{-1}: Sukhorukov *et al.*[17] assign this phenomenon to the formation of a crystalline structure of the compound; according to Ichikawa[18] two vibration bands above 2000 cm^{-1} can be associated to the presence of cyanamide $[N–C{\equiv}N]^{2-}$ and isocyanamide $[N-N{=}C]^{2-}$ groups. The isocyanamide group has a longer C=N bond length (0.016 Å) than cyanamide. The cluster size also influences the bond length.[19] Berger *et al.*[15] comparing the IR spectra of $MgCN_2$, $SrCN_2$ and $BaCN_2$ observed the splitting for $SrCN_2$. According to them, this splitting is the result of two crystallographically independent nitrogen atoms in the cyanamide ion. The splitting of the band at about 2000 cm^{-1} is also observed for lead cyanamide[20] which has two C–N bond lengths significantly different.[21] However, in this case it is justified that the two C–N bond lengths in cyanamide group are different because these are single and triple bonds.

In Table 5 we report a few bibliographic data for the alkaline-earth metal cyanamides compared with the lead cyanamide and our cadmium cyanamide. According to these data we observe that the M–N bond lengths increase for alkaline-earth metals and they are associated with the decrease of C–N bond lengths in the cyanamide group. Therefore, the vibrational frequencies characteristic of triple bonds in the cyanamide anion shift toward lower values. In this case, the increase of M–N bond lengths is mainly due to the increase of M^{2+} size since the alkaline-earth metal cations have almost the same electronegativity.

On the other hand, cadmium and lead display a larger electronegativity[22] than the previous alkaline-earth metals,

Table 5 Bibliographic data for H_2CN_2 and a few cyanamide salts compared with our $CdCN_2$. M^{2+}-metal ion

Compound and symmetry group	Ionic radius[a,25] for M^{2+}/Å	M–N bond length/Å	Bond length/Å between C and N in $[N(2)–C{\equiv}N(1)]^{2-}$	C≡N stretching vibration/cm^{-1}	Atomic mass of M	$\Delta\chi$ for M–N	Ref.
$MgCN_2$ $R\bar{3}m$	0.72	2.190	1.248	2114	24.30	1.8	15
$CaCN_2$ $R\bar{3}m$	1.00	2.461	1.224	2032	40.08	2.0	24
$SrCN_2$ *Pnma*	1.18	2.622, 2.658, 2.602, 2.643	1.222 (N1), 1.228 (N2)	2023, 1989	87.62	2.0	15
$BaCN_2$ $R\bar{3}c$	1.35	2.774, 2.843, 2.867	1.192	1947	137.34	2.1	15
$CdCN_2$ $R\bar{3}m$ or $R3m$	0.95	2.377	1.205 or 1.04 (N1), 1.36 (N2)	2113	112.41	1.3	This work
$PbCN_2$ *Pnma*	1.19	2.31,[21] 2.62	1.156 (N1),[21] 1.297 (N2)	2000,[20] 1930	207.19	1.2	20, 21
H_2CN_2	—	—	1.15 (N1), 1.31 (N2)	2225	—	0.8	23

[a]Effective ionic radius for coordination number = 6; $\Delta\chi$: difference of electronegativity in Pauling unity.

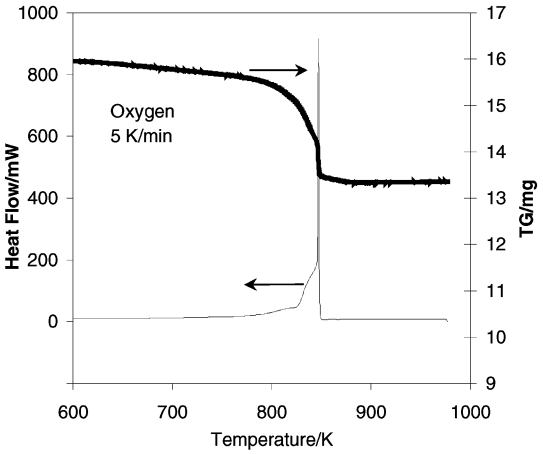

Fig. 7 TG–DSC for cadmium cyanamide.

thus the ionic character of Cd–N and Pb–N bonds is probably smaller. This fact must influence the length of the C–N bonds in the cyanamide group. Moreover, it is well known that the frequency shift in an infrared spectrum also depends on the cation masses *i.e.* change from cadmium to lead. This effect is even more visible (Table 5) when we compare lead cyanamide[20] to cyanamide H_2CN_2.[23]

The data in Table 5 show that the splitting of the vibration band at about 2000 cm^{-1} is not observed for linear compound structures like $MgCN_2$,[15] $CaCN_2$,[24] H_2CN_2[23] and $CdCN_2$.

Thermogravimetry

Fig. 7 shows the thermogravimetric results obtained under an oxygen stream. We observe the beginning of the weight loss at about 573 K and a sharp weight loss is noticed above 773 K. The red-brown final residue is identified by XRD as CdO (JCPDS 05-0640). The weight loss recorded in the experience corroborates also the CdO formation. It can be supposed that the decomposition of our cadmium cyanamide occurs according to the reaction proposed by Bolis-Cannella for air-annealed $CdCN_2$:[1]

$$CdCN_2 + 3/2O_2 \rightarrow CdO + CO_2 + N_2$$

The enthalpy and the transformation temperature determined in our experience are respectively -534.7 kJ mol^{-1} and 827 K.

It seems that the behaviour of our cadmium cyanamide with the temperature is similar to that observed by Uritskaya *et al.*[2] for air-annealed samples. They found traces of cadmium cyanamide (by infrared analysis) and they identified CdO (by XRD) after air-annealing at 773 K.

These observations are not completely in agreement with those reported by Bolis-Cannella[1] where the $CdCN_2$ oxidation under air begins at 573 K and is complete at 673 K.

Conclusion

In this work we described a new phase of cadmium cyanamide obtained by chemical bath deposition. TEM analyses of cadmium cyanamide show a nanocrystalline powder with very complex shape. This observation is in agreement with the anisotropic broadening observed in the X-ray diffraction pattern. We performed the structure refinement by the Rietveld method within 2 trigonal space groups $R\bar{3}m$ and $R3m$. The assignement of the $R3m$ space group to cadmium cyanamide gives a better agreement with our FTIR results. Furthermore, we determined the temperature and the enthalpy of cadmium cyanamide transformation under oxygen by thermogravimetric analysis.

Acknowledgements

The authors are grateful to Professor Jan Kusinski of the University of Mining and Metallurgy in Cracow (Poland) for his experimental assistance in characterisation of the samples by TEM. We thank also Dr P. Gemeiner for the FTIR measurements and G. Boemare (LSPMS/ECP) for TG-DSC analyses.

Research funded in the framework of JOULE III Programme, contract JOR-CT-97-0124

References

1 C. Bolis-Cannella, *Ann. Chim.*, 1954, **44**, 1050.
2 A. A. Uritskaya, V. P. Panov, N. D. Betenekov, I. I. Polezhaev, G. D. Sizova and G. A. Kitaev, *Neorg. Mater.*, 1976, **12**, 193.
3 V. P. Medvedev, L. G. Skornyakov, N. D. Betenekov, T. A. Drozdova, G. A. Kitaev and L. A. Brusnitsyna, *Neorg. Mater.*, 1978, **14**, 1793.
4 G. A. Kitaev, T. P. Bol'shchikova and L. E. Yatlova, *Zh. Neorg. Khim.*, 1971, **16**, 3173.
5 V. I. Dvoinin, L. G. Skornyakov, L. E. Yatlova, M. V. Degtyarev and G. A. Kitaev, *Zh. Prikl. Khim.*, 1982, **55**, 213.
6 A. Kylner, J. Lindgren and L. Stolt, *J. Electrochem. Soc.*, 1996, **143**, 2662.
7 A. Kylner and M. Wirde, *Jpn. J. Appl. Phys.*, 1997, **36**, 2167.
8 A. Kylner, *J. Electrochem. Soc.*, 1999, **146**, 1816.
9 B. Malinowska, M. Rakib and G. Durand, *Prog. Photovoltaics*, 2001, **9**, 389.
10 B. Malinowska, M. Rakib and G. Durand, *Prog, Photovoltaics*, in the press.
11 B. Malinowska, M. Rakib and G. Durand, *Sol. Energy Mater. Sol. Cells*, submitted for publication.
12 J.-F. Berar, G. Calvarin and D. Weigel, *J. Appl. Crystallogr.*, 1980, **13**, 201.
13 J.-F. Berar and G. Baldinozzi, *CPD Newslett.*, 1998, **20**, 3.
14 G. K. Williamson and W. H. Hall, *Acta Metall.*, 1953, **1**, 22.
15 U. Berger and W. Schnick, *J. Alloys Compd.*, 1994, **206**, 179.
16 A. Kylner, A. Rockett and L. Stolt, *Diffus. Defect Data, Pt. B*, 1996, **51–52**, 533.
17 B. I. Sukhorukov and A. I. Finkel'shtein, *Opt. Spectrosk.*, 1959, **7**, 393.
18 K. Ichikawa, Y. Hamada, Y. Sugawara, M. Tsuboi, S. Kato and K. Morokuma, *Chem. Phys.*, 1982, **72**, 301.
19 T. Lower, G. A. Bowmaker, J. M. Seakins and R. P. Cooney, *Chem. Mater.*, 1997, **9**, 967.
20 R. A. Nyquist and R. O. Kagel, *Handbook of infrared and Raman spectra of inorganic compounds and organic salts*, vol. 4, p. 72.
21 X. Liu, A. Decker, D. Schmitz and R. Dronskowski, *Z. Anorg. Allg. Chem.*, 2000, **626**, 103.
22 R. G. Pearson, *J. Am. Chem. Soc.*, 1963, **85**, 3533.
23 Z. V. Zvonkova and A. N. Khvatkina, *Sov. Phys. Crystallogr.*, 1961, **6**, 147.
24 N.-G. Vannerberg, *Acta Chem. Scand.*, 1962, **16**, 2263.
25 R. D. Shannon, *Acta Crystallogr., Sect. A*, 1976, **32**, 751.